LIDAR system for monitoring turbulence profiles

Gary G. Gimmestad, David A. Roberts, John M. Stewart, Jack W. Wood
Georgia Tech Research Institute
Atlanta, GA, USA 30332-0834

ABSTRACT

We have developed a new type of lidar for measuring range profiles of atmospheric optical turbulence. The lidar is based on a measurement concept that is immune to artifacts caused by effects such as vibration or defocus. Four different types of analysis and experiment showed that a turbulence lidar that can be built from commercially available components would attain a demanding set of performance goals. Preliminary data shows that the lidar is operating properly. The lidar is scheduled for testing with truth data in October 2007.

1. INTRODUCTION

We have developed a new type of lidar (light detection and ranging) technique in order to measure the strength of refractive turbulence $C_n^2(h)$. Over the past 25 years, several techniques have been proposed for laser remote sensing of C_n^2 profiles. Most of the techniques were based on efforts to measure the effects of turbulence on a laser beam, such as beam wander or beam broadening. Such techniques are sensitive to instrumental problems, such as defocus and vibrations, which create artifacts that appear exactly the same as the effects of the atmosphere. In 1998-99, we developed a much better approach based on differential image motion that we call Differential Image Motion Lidar, or *DIM Lidar*, and showed that it is free of the artifacts mentioned above [1,2]. DIM Lidar can be described as a hybrid of two well-established astronomical techniques: the Differential Image Motion Monitor, which uses light from natural stars to measure the integrated effect of atmospheric turbulence in terms of Fried's coherence parameter r_0, and laser guide star adaptive optics, in which a laser beam is used to create an artificial beacon at a fixed altitude by focusing the beam and range gating an imager. By moving the guide star through a range of altitudes the DIM profile can be traced out, and an inversion algorithm can be used to retrieve the C_n^2 profile.

The DIM technique measures the variance of the differential wavefront tilt at two spatially separated apertures. In the focal plane, changes in tilt correspond to image motion, which is why the name of the astronomical instrument incorporates the phrase "differential image motion." This phrase is also incorporated into the name DIM Lidar, and the notation σ_{DIM}^2 is used throughout this paper to mean the DIM variance.

We performed field experiments at Georgia Tech in 1999 using a hard target instead of atmospheric backscatter and showed that the technique yields values for path-averaged C_n^2 that are the same as a scintillometer. This was a promising result, but it did not answer the basic questions of how accurately a DIM Lidar can measure $C_n^2(h)$ and with what time and space resolutions. The work described in Sections 3 - 6 of this paper answered these questions. A combination of analysis, field measurements, development and testing of new inversion algorithms, and wave optics simulations was used.

The performance goals for the first DIM Lidar were to measure $C_n^2(h)$ within a factor of two in the range 10^{-18} to 10^{-12} $m^{-2/3}$ from the ground to 10 km altitude, with 10-minute averaging, during both day and night. The DIM Lidar is scheduled for testing against truth data during October 2007.

2. THEORY

Because the DIM LIDAR measures differential wavefront tilt in the same manner as a standard astronomical instrument, much of the analytical model can be adapted from previous work. Eaton et al. [3] presented an early

analysis of differential image motion, for the application of a stellar seeing monitor. Sarazin and Roddier [4] later presented a derivation that treated the two axes of motion separately. In both analyses, an algorithm is presented from which we can derive an equation of the form

$$\sigma_{DIM}^2 = f(d/D)D^{-1/3}\,\overline{C}_n^2, \text{ where} \tag{1}$$

σ_{DIM}^2 is the variance of the differential image motion (radians^2)
f is a function,
D is the subaperture diameter (m),
d is the subaperture separation (m), and the path-integrated turbulence is defined by

$$\overline{C}_n^2 = \int_0^S C_n^2(s)(1-s/S)^{5/3}ds, \text{ where} \tag{2}$$

S is the distance to the laser guide star.

The only difference between the two published analyses is in the function of d/D. Eaton et al. derived the result that

$$r_0 = \left[\frac{27.5}{k^2 d^{1/3}\sigma^2}\left(1-\frac{25}{36}(d/D)^{1/3}\right)\right]^{3/5}, \text{ where} \tag{3}$$

$k = 2\pi/\lambda$, and
λ is the wavelength (m).

In the astronomical scenario, r_0 is related to $C_n^2(h)$ by Eq. (3). For our case, in which the source is at a finite distance, we must include a path weighting function in the integral. In this case, for vertical viewing,

$$r_0 = \left[0.42k^2\overline{C}_n^2\right]^{-3/5} \tag{4}$$

Using Eq. (4) in Eq. (3) and solving for σ_{DIM}^2, we find that Eaton's function of d/D can be written

$$f(d/D) = 33.2\left[0.349 - 0.242(d/D)^{-1/3}\right]. \tag{5}$$

Again for the astronomical DIM instrument, Sarazin and Roddier [4] derived the relations

$$\sigma_l^2 = 2\lambda^2 r_0^{-5/3}[0.179D^{-1/3} - 0.0968d^{-1/3}] \text{ and} \tag{6a}$$

$$\sigma_t^2 = 2\lambda^2 r_0^{-5/3}[0.179D^{-1/3} - 0.145d^{-1/3}] \tag{6b}$$

where the subscripts l and t refer to longitudinal and transverse motion. Using the same definitions as for Eaton, we find that these expressions become

$$\sigma_l^2 = f_l(d/D)D^{-1/3}\,\overline{C}_n^2 \text{ and} \tag{7a}$$

$$\sigma_t^2 = f_t(d/D)D^{-1/3}\overline{C}_n^2 . \tag{7b}$$

Note that the total DIM is given by $\sigma_{DIM}^2 = \sigma_l^2 + \sigma_t^2$, so

$$. \ \sigma_{DIM}^2 = f(d/D)D^{-1/3}\,\overline{C}_n^2 \tag{8}$$

where

$$f(d/D) = 33.2\left[0.358 - 0.242(d/D)^{-1/3}\right], \tag{9}$$

which can be seen by inspection to be very close to Eaton's result. Equations 3, 4, and 9 were the basis for the analysis presented in the next section, and they also constitute the *forward model* for the development of inversions, i.e. the analytic expression relating a given $C_n^2(h)$ profile to the value of σ_{DIM}^2 that would be expected for a given altitude of the laser guide star, for the instrumental parameters d and D.

3. ANALYSIS

The purpose of the analysis was to design a turbulence lidar based on commercially available components that can reach the performance goals listed at the end of Section 1. The initial design was in terms of system parameters only. As shown by Eqs. 3 and 4, σ_{DIM}^2 depends only on the altitude, turbulence profile, subaperture diameter, and subaperture separation. Differential image motion is calculated from image positions in the focal plane, and the positions are taken to be the image centroids. For this reason, it is important to ensure that the variance in the image centroid positions due to the measurement process is small relative to the expected variance caused by atmospheric turbulence. Morgan et al. [5] showed that the accuracy with which an image centroid can be found depends on the image size, the number of photoelectrons in the image, and the numbers of sky background photoelectrons and read-out noise electrons in the image. The image size was calculated for a set of altitudes by using Gaussian beam theory to find the beam waist diameter at the range of the scattering volume and then modifying it to find the short-exposure image size in the focal plane, based on the turbulence profile along the laser beam path. The numbers of laser and sky photoelectrons in the image were found by using the lidar equation and an equation describing the received power due to sky radiance. Finally, the variance of the image centroid position error was calculated as a function of range. The analysis was performed for a laser wavelength of 355 nm and for atmospheric parameters including $C_n^2(h)$, visibility, the scale height, the Angstrom coefficient, the sky radiance, and the lidar extinction-to-backscatter ratio. The DIM Lidar was designed, using the specifications of commercial components, so that the centroiding error variance will always be small compared to the image motion variance caused by atmospheric turbulence.

In order to optimize the lidar design for planned verification tests at the White Sands Missile Range (WSMR) in New Mexico, it was necessary to adopt a set of turbulence profiles that covered a range of conditions from daytime with a well-developed convective boundary layer to stable nighttime. Three WSMR profiles were adapted from graphs in the IR Handbook [6]:a morning profile measured at 0904 MST in the winter, a midday profile measured at 1319 MST in the summer, and a night profile measured at 2100 MST. All three were extended to 20 km above sea level with the Hufnagle-Valley 5/7 model ($HV_{5/7}$). The $HV_{5/7}$ model itself was also used as a profile.

The analysis showed that the set of system parameters listed in Tables 1 and 2 is adequate to reach the performance goals, and a DIM Lidar with those parameters has been built. The system also includes a conventional aerosol backscatter lidar in order to record the distribution of aerosols along the beam path.

Table 1. Transmitter Parameters

Parameter	Value
Laser type	Nd:YAG
Wavelength	355 nm
Pulse Energy	350 mJ
Pulse Repetition Frequency	50 Hz
Pulse Width	3-7 ns
Raw Beam Divergence	650 urad to $1/e^2$ intensity level
Raw Beam Diameter	0.7 mm to $1/e^2$ intensity level
Output Beam Divergence	15 – 150 urad to $1/e^2$ intensity level
Output Beam Diameter at Transmitter	44 mm to $1/e^2$ intensity level
Transmitter Aperture Location	Centered on receiver primary mirror behind secondary mirror

Table 2. Receiver Parameters

Parameter	Value
Primary Mirror Diameter	406.4 mm
Secondary Mirror Diameter	152.4 mm
Telescope Prime Focal Length	3414 mm
Telescope Prime Focus Image Scale	3.41 microns per microradian
Prime Focus Diffraction Spot Size	7.3 microns (2.13 urad) at 355 nm
Optical Bandpass	10 nm FWHM centered at 355 nm
System Transmission	25% minimum
Camera Array Format	80 X 80 pixels, 24 um pitch, 100% fill factor
Array Quantum Efficiency	60% at 355 nm
Array Readout Noise per Pixel	4.1 e^- at 50 Hz frame rate and max gain
DIM Aperture Diameters	76.2 mm maximum
Number of DIM Apertures	Four
Aperture Arrangement	Equally spaced on 317.5 mm diameter circle
DIM Channel Effective Focal Length	3414 mm
DIM Channel Image Scale	3.41 microns per microradian

4. FIELD MEASUREMENTS

As mentioned above, we had performed previous field measurements in 1999 to demonstrate that the DIM method yields the same path-averaged value of C_n^2 as a conventional scintillometer on a fixed horizontal path. In order to perform those measurements at low cost, we developed a system that we called a *hard-target analog* of a DIM Lidar. A CW HeNe laser beam was expanded and focused on a white target board at 300 m range, and a fast-framing digital imager was used in the receiver to acquire large sets of images from a two-aperture receiver. The hard-target analog experiment avoided the costs associated with range-gated imaging and relying on atmospheric backscatter, but it did not demonstrate that the DIM method could be used to measure altitude profiles in which C_n^2 was variable, and it did not address inversion of the DIM data to find turbulence profiles. In order to address these shortcomings, new hard-target analog measurements were performed on slant paths in the project described here, during November 2004 [7].

The new set of field measurements was undertaken with a new version of the CW lidar on a tracking mount. Truth data were acquired by raising and lowering micro-thermal probes on a large balloon that also served as a target for the laser beam. One complete ascent and descent of the balloon required at least one hour, so our goal was to obtain data sets during times when the turbulence profile might be fairly constant in time, such as during mid-afternoon. Unfortunately, the field measurements were interrupted by an accidental release of the balloon and data were

acquired only during times when the atmosphere was rapidly changing. Reasonable agreement between the measured and predicted values of differential image motion was obtained, as shown in Fig. 1., but the data were not appropriate for inversion because the truth data did not accurately represent the rapidly-changing turbulence profile.

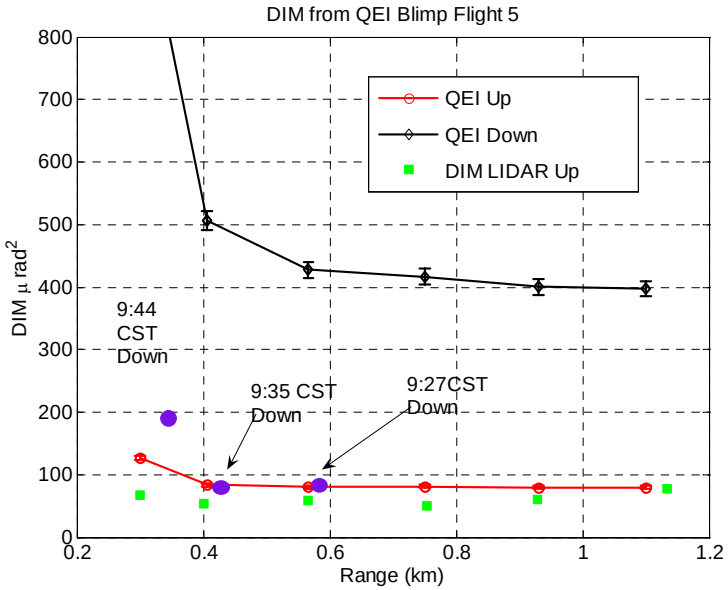

Figure 1. Measured and predicted DIM profiles

The scatter in the field test data was shown to agree with the theory presented by Andreas [8], who analyzed the maximum rate at which statistically independent measures of turbulence can be obtained with various instruments. We used Andreas' analysis to show that the rate is about 50 Hz for the DIM Lidar, and this rate sets a fundamental limit on the accuracy with which estimates of σ^2_{DIM} can be obtained in a given time. For example, ten minutes is typically taken as the maximum time that the atmosphere can be assumed to be constant. At 50 Hz, ten minutes corresponds to 30,000 image frames, and these frames must be allocated among the laser guide star altitudes. In this study, we assumed that 4,000 frames would be recorded at each of seven altitudes for a total of 28,000 frames in a ten-minute data set (some time must be allowed for re-focusing at each altitude). The expected r.m.s. fractional uncertainty in a variance estimate is given by Frieden [9] as

$$\frac{\delta\sigma^2}{\sigma^2} = \sqrt{\frac{2}{N-1}} \tag{9}$$

where N is the number of samples. Note that this uncertainty applies to both the longitudinal and transverse axes of image motion, so for the DIM LIDAR the uncertainty is given by

$$\frac{\delta\sigma^2_{DIM}}{\sigma^2_{DIM}} = 2\sqrt{\frac{1}{N-1}} \tag{10}$$

which yields an r.m.s. uncertainty of 3% for 4,000 image frames. There are three requirements for Eq. (9) to be valid: 1) the statistics of the atmosphere must be stationary during the measurement time interval; 2) the samples must be statistically independent; and 3) the random variable σ^2_{DIM} must follow the normal probability law.

5. INVERSION ALGORITHMS

Equations 1 and 2 can be rewritten as

$$\sigma^2_{DIM}(h) = A\int_0^h C_n^2(h')(1-h'/h)^{5/3}dh' \tag{11}$$

Where h is the distance from the receiver and A is a constant dependent on geometry of the receiver. Because the measurements will be performed at a discrete set of altitudes, the integral in Eq. (11) is replaced with a summation in practice, and the equation can then be inverted with standard matrix techniques [10]. Unfortunately, the matrix inversion method of finding $C_n^2(h)$ suffers from high noise gain. A graph of the weighting function in the integral of Eq. (20) has a classic shape that always leads to ill-conditioned problems [11], which means that small uncertainties in the input data, and even the act of discretizing the problem, cause large changes in the output including oscillations and negative values. A more subtle approach is needed. By differentiating Eq. (11), we obtain a different weighting function that results in a very low noise gain. We refer to this approach as the *slope inversion method*. Taking the derivative of both sides of Eq. (20) with respect to h we obtain

$$S(h) = \int_0^h C_n^2(h')[\tfrac{5}{3}h'(1-h'/h)^{2/3}/h^2]dh'. \tag{12}$$

The weighting functions for the original equation and the slope method are plotted in Fig. 2. To obtain the function *S*(*h*) from experimental values of σ^2_{DIM}, a suitable analytic function for $\sigma^2_{DIM}(h)$ can be fitted to the experimental values. Since $C_n^2(h)$ is non-negative, $\sigma^2_{DIM}(h)$ will be always be constant or increasing. Further, since $\sigma^2_{DIM}(h)$ is related to the turbulence profile by Eq. (12) it will always be zero at zero range and it will be smoothed by the integral and weighting function.

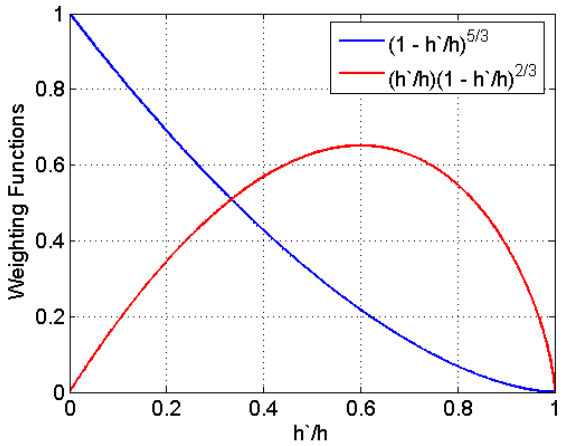

Figure 2. The weighting functions of the original and the slope method equations.

Not all functions representing $\sigma^2_{DIM}(h)$ correspond to realizable profiles of turbulence. For example, some may generate profiles where $C_n^2(h)$ is negative. One way to find analytical functions *M(h)* is to solve for the integral in Eq. (20) for distributions of $C_n^2(h)$ that are commonly used in models. A function that approximately provides a decreasing exponential for $C_n^2(h)$ is

$$M(h) = h/(h+b) \tag{22}$$

and a function that approximates a Gaussian layer in $C_n^2(h)$ is

$$M(h) = [h/(h+b)]^2 \tag{23}$$

Further, a constant $M(h)$ corresponds to a delta function in $C_n^2(h)$ at h=0. This function may be used to approximate a ground layer that is thin compared to the lowest h value for which M is measured. Combining these provides a DIM function that encompasses all these features:

$$M(h) = M_0 + M_1 h/(h+b_1) + M_2[h/(h+b_2)]^2 \tag{24}$$

where M_0, M_1, M_2, b_1, and b_2 are constants. This function corresponds quite closely to the Kukharets and Tsvang model for daytime convective boundary layer $C_n^2(h)$ profiles that has been used effectively at WSMR [6]. Twenty retrievals of the $HV_{5/7}$ profile with random noise added are shown in Fig. 3 to illustrate the stability of the inversion.

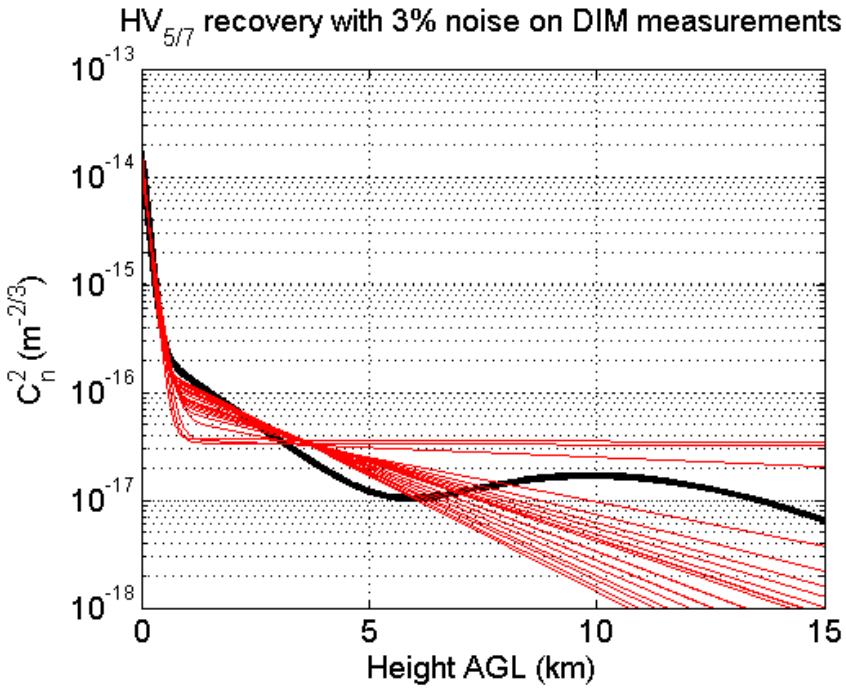

Figure 3. Retrieval of $HV_{5/7}$ profiles with added noise.

6. WAVE OPTICS SIMULATIONS

The DIM Lidar's performance depends on its ability to find the centroids of images of the laser guide star. The system was designed so that the variance of centroiding errors will always be much less than the variance of the differential image motion. However, the analysis entailed several approximations:

- Gaussian laser beam propagation theory was used to find the beam waist diameter at each range in the absence of turbulence,
- Laser beam broadening by turbulence was approximated by a constant value for all laser pulses at each range, for each turbulence profile,

- Scattering of the laser light by aerosols and molecules over an extended range was modeled as scattering from a diffuse target plus defocus blurring, and

- The laser beacon image profile in the system's focal plane was always represented by a simple Gaussian function.

The objective of the wave optics simulations was to quantify any errors in the calculations of the system's expected centroiding accuracy caused by the approximations listed above. The Optical Sciences Company (tOSC) performed the wave optics simulations under subcontract to GTRI, and the results of their simulations are briefly summarized in this section.

The system parameters listed in Tables 1 and 2 were used in the wave optics simulations. The laser beam was propagated through turbulence phase screens to each laser guide star altitude with the beam diameter minimized at each altitude. The combination of the laser pulse's inherent intensity distribution and the distorting effects of the turbulence phase screens determine the resulting guide star intensity distribution. The image of the guide star was found by convolving the turbulence-distorted laser pulse at the guide star altitude with the image of a point source placed at the same altitude. The simulations were extensive - five thousand turbulence samples were used and five thousand intensity centroids were generated for each range and each of the receiver apertures, for each of the three profiles. Differential tilt variances between the subapertures were compared to values produced by using Eqs. (1), (5), and (11).

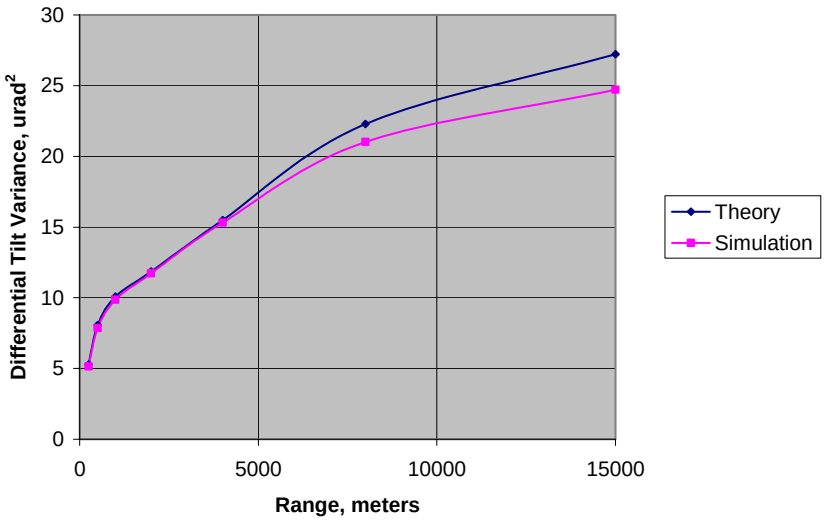

Figure 4. Theoretical and wave-optics simulated differential tilt variances for the morning profile

The theoretical values of the differential tilt variance are shown in Fig. 4 along with those generated by the simulation, for the morning profile. All three profiles showed similar agreement between simulation and theory, except at very long ranges where the laser beam diameter becomes comparable to the separation between the subapertures and Eq. (2) no longer describes the geometry correctly.

7. CONCLUSIONS

We are developing a new type of lidar, known as the DIM Lidar, for measuring range profiles of turbulence. An analysis showed that a demanding set of performance goals can be met with a lidar system built from commercially-available components. Field measurements of DIM were conducted on slant paths through the atmosphere, from the ground to a tethered blimp, with truth data measured by an instrument package carried by the blimp. The resulting DIM data showed satisfactory agreement with predictions based on the analysis. A stable inversion method was developed and a set of well-behaved functions was found to represent DIM. Finally, wave optics simulations were

carried out and the results agreed with the simpler analysis except at the longest ranges. The four research efforts described above all indicate that the DIM Lidar will perform as expected. A brassboard version of the DIM Lidar has been constructed, and tests against truth data are scheduled for October 2007.

ACKNOWLEDGEMENTS

The authors acknowledge the assistance of Mike Jensen at QEI Technologies of Denver, Colorado, Robert Stovall and Rick Welch of the 46th Test Wing at Eglin Air Force Base, Florida, David L. Fried, consultant, Glenn Tyler and Michael Campbell of tOSC, and Ian Gatland, Professor Emeritus in the Physics Department at Georgia Tech.

The project is funded under the DTRMC DE T&E/S&T Program. The Executing Agent is Minh Vuong of U.S. Army PEO-STRI in Orlando, Florida.

REFERENCES

1. M.S. Belen'kii, D.W. Roberts, J.M. Stewart, G.G. Gimmestad, and W.R. Dagle, Experimental validation of the differential image motion lidar concept, *Optics Letters* Vol. 25, 518-520, (2000).

2. M.S. Belen'kii, D.W. Roberts, J.M. Stewart, G.G. Gimmestad, and W.R. Dagle, Experimental validation of the differential image motion lidar concept, Proc. SPIE Vol. 4377, 307-316 (2001).

3. F.D. Eaton et al., Comparison of two techniques for determining atmospheric seeing, *Proc. SPIE* Vol. 926, 319-334 (1988).

4. M. Sarazin and F. Roddier, The ESO Differential Image Motion Monitor, Astronomy and Astrophysics Vol. 227,294-300 (1990).

5. J.S. Morgan, D.C. Slater, J.G. Timothy, and E.B. Jenkins, Centroid Position Measurements and Subpixel Sensitivity Variations with the MAMA Detector, *Applied Optics* Vol. 28, 1178-1192 (1989).

6. F.G. Smith, Ed., *The Infrared and Electro-Optical Systems Handbook* Vol. 2, Atmospheric Propagation of Radiation (1993).

7. G.G. Gimmestad, M.W. Dawsey, D.W. Roberts, J.M. Stewart, J.W. Wood, F.D. Eaton, M.L. Jensen, and R.J. Welch, Field Validation of Optical Turbulence Lidar Technique, Proc. SPIE Vol. 5793, 10-16 (2005).

8 E.L. Andreas, Estimating Averaging times for Point and Path-Averaged Measurements of Turbulence Spectra, *J. App. Meteor*. Vol. 27, 295-304 (1988).

9. B. R. Frieden, *Probability, Statistical Optics, and Data Testing*, 3rd Edition, Springer, New York, p. 256 (2001).

10. C.D. Rodgers, *Inverse Methods for Atmospheric Sounding – Theory and Practice*, World Scientific, Singapore (2000).

11. S. Twomey, *Introduction to the Mathematics of Inversion in Remote Sensing and Indirect Measurements*, Dover, New York, (1977).